Investigation of the Proton Release Channel of Bacteriorhodopsin in Different Intermediates of the Photo Cycle. A Molecular Dynamics Study

Jochen Nagel,*,‡ Olle Edholm,§ Oliver Berger,‡ and Fritz Jähnig‡,||

Max-Planck-Institut für Biologie, Abteilung Membranbiochemie, Corrensstrasse 38, D-72076 Tübingen, Germany and Royal Institute of Technology, Department of Theoretical Physics, S-10044 Stockholm, Sweden

Received September 26, 1996; Revised Manuscript Received January 7, 1997⊗

ABSTRACT: Molecular dynamics simulations on bacteriorhodopsin were performed starting from a conformation based on electron cryomicroscopy studies [Henderson, R., et al. (1990) *J. Mol. Biol. 213*, 899−929]. We examined the proton release channel in different intermediates of the bacteriorhodopsin photocycle. In the simulations of the ground state, two stable sets of conformations were observed differing in the distance of the guanidinium group of Arg82 to the Schiff base. The set of conformations in which Arg82 is located closer to the Schiff base has a lower potential energy and agrees better with experimental data than the other set. With both sets, we performed a series of simulations in which the chromophore was isomerized to different states using purposive and nonpurposive methods. The energetic consideration of the different states argues for the location of the guanidinium group of Arg82 close to the Schiff base. The results also show that no $C_{13}-C_{14}$, $C_{14}-C_{15}$ dicis conformation of the retinal occurs in the K/L-intermediate of the photocycle instead supporting the occurrence of $C_{13}-C_{14}$ cis in these intermediates. In a last series of simulations, we modeled the M-intermediate of the bacteriorhodopsin photocycle. Again, comparison to different experimental data indicates that Arg82 points toward the Schiff base. We conclude that the guanidinium group of Arg82 is located close to the Schiff base at a distance of approximately 4.5 Å and stays there at least up to the M-intermediate of the photocycle.

Bacteriorhodopsin (BR)[1] is one of the best characterized membrane proteins [for reviews, see Birge (1990), Mathies et al. (1991), and Oesterhelt et al. (1992)]. A structural model based on electron cryomicroscopy (ECM) and other data has been developed and has permitted to get insight into its function as a light driven proton pump (Henderson et al., 1990; Grigorireff et al., 1996). The structure of BR consists of seven membrane-spanning alpha-helices arranged in a kidney-shaped manner. In the interior of the kidney there is a retinal which is bound to Lys216 via a Schiff base (SB) and which acts as a chromophore. In the ground state the SB is protonated and the retinal has an all-trans configuration (Figure 1a) with an absorption maximum at 568 nm (BR_{568}). In the absence of light, BR relaxes to the dark-adapted state which is a 2:1 mixture of BR_{555} and BR_{568} (Scherrer et al., 1989; Song et al., 1995). BR_{555} contains a $C_{13}-C_{14}$ cis, $C_{15}-N$ syn retinal (Smith et al., 1984; see Figure 1b). Illumination of the dark-adapted state shifts the balance to the all-trans state. Light absorption in the all-trans state initiates a photocycle which leads to the translocation of one proton per absorbed photon from the cytoplasmic to the extracellular side of the membrane. During the cycle, retinal undergoes isomerization reactions and changes its protonation state.

Apart from the SB, three other interior amino acids of the proton release channel are charged in the ground state: Arg82, Asp85, and Asp212. Asp85 is the proton acceptor from the SB in the M-intermediate of the photocycle and stays protonated until the end of the cycle (Hessling et al., 1993). Asp212 is deprotonated during the whole photocycle and is discussed to take part in the complex counterion for the SB in the ground state (Fahmy et al., 1993). The role of Arg82 is less clear, but mutation experiments showed that in the absence of Arg82 proton release to the extracellular medium is slowed down (Balashov et al., 1993). It was suggested that the long side chain of Arg82 acts as a proton lift in BR and releases the proton (Mathies et al., 1991). Recently, however, the proton release group has probably been identified as Glu204 (Scharnagl et al., 1994; Scharnagl et al., 1995; Brown et al., 1995b), and Scharnagl et al. (1994, 1995) suggested that Arg82 mediates the changes near the SB to Glu204. However, the orientation of Arg82 and therefore the structure of the proton release channel in the different intermediates of the photocycle is still not known exactly. In the model structure of Henderson et al. (1990) and in the refined model structure (Grigorieff et al., 1996), Arg82 points toward the extracellular side, the distance between the guanidinium group of Arg82 and the SB nitrogen is 11.5 Å (Figure 2a). But even in the refined model of BR, the authors emphasized that the orientation of the side chain of Arg82 is still unclear, because no clear electron density of this side chain could be observed. Bashford and Gerwert (1992) suggested on the basis of p*K* calculations that Arg82 should be rotated in such a way that its guanidinium group points toward Asp85 with a distance of 7.5 Å to the SB (Figure 2b). Edholm et al. (1995) performed molecular dynamics (MD) simulations on BR starting from

* To whom correspondence should be addressed.
‡ Max-Planck-Institut für Biologie.
§ Royal Institute of Technology.
|| Deceased on June 16th, 1996.
⊗ Abstract published in *Advance ACS Abstracts,* February 15, 1997.
[1] Abbreviations: BR, bacteriorhodopsin; SB, Schiff base; ECM, electron cryomicroscopy; MD, molecular dynamics; cpuh, central processor unit hour; rms, root-mean-square; rmsd, root-mean-square deviation.

S0006-2960(96)02427-0 CCC: $14.00

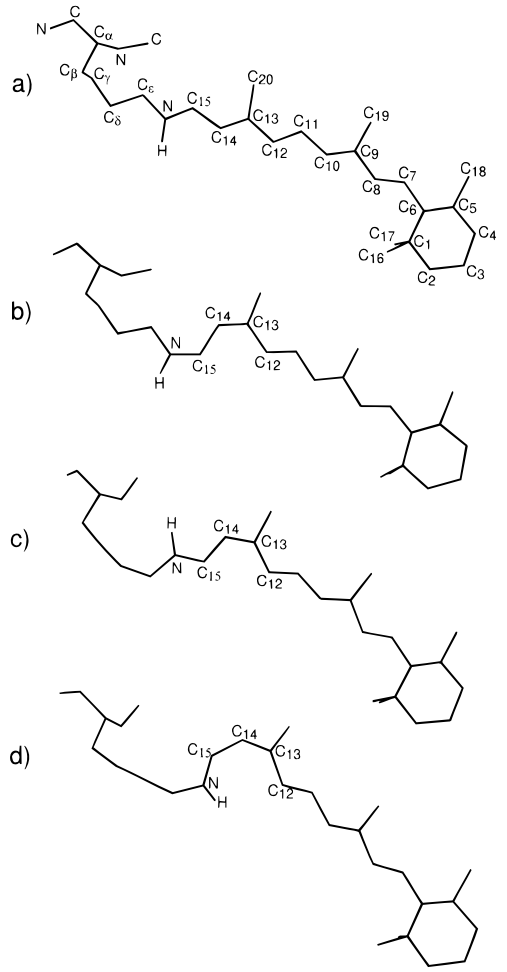

FIGURE 1: Lys216 and retinal in different states: (a) all-trans state; (b) $C_{13}-C_{14}$ cis, $C_{15}-N$ syn state; (c) $C_{13}-C_{14}$ cis state; (d) $C_{13}-C_{14}$, $C_{14}-C_{15}$ dicis state.

the model structure of Henderson et al. (1990) with Arg82 rotated to the position suggested by Bashford and Gerwert (1992) in which the orientation of Arg82 was quite stable, but in most of the MD runs a further rotation of Arg82 toward the SB up to a distance of 4.5 Å was observed (Figure 2c). Knowledge of the real orientation of Arg82 would shed light into the understanding of the proton release. The primary aim of our work was to elucidate this important topic in the ground state of BR and in the first intermediates of its photocycle.

There are still contradictory opinions about the retinal conformations in the first steps of the photocycle. Schulten et al. (1984) proposed a photocycle with a primary photo reaction from all-trans to $C_{13}-C_{14}$, $C_{14}-C_{15}$ dicis (Figure 1d) followed by reisomerization of $C_{14}-C_{15}$ to trans during formation of the M-intermediate. In comparison, Fodor et al. (1988) proposed the C-T model in which the retinal occurs only in all-trans and in $C_{13}-C_{14}$ cis (Figure 1c). Unfortunately, experimental data concerning the behavior of $C_{14}-C_{15}$ are ambiguous. The results of theoretical investigations are ambigous, too. Nonella et al. (1991) and Zhou et al. (1993) argued in favor of the existence of a $C_{13}-C_{14}$, $C_{14}-C_{15}$ dicis state whereas Engels et al. (1995) found arguments supporting the C-T model. Our second aim was to describe conformation and orientation of the retinal in the different intermediates.

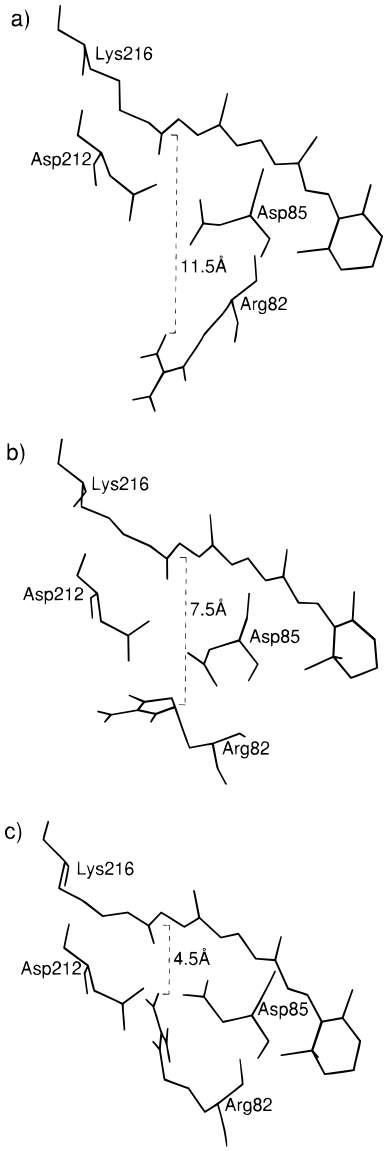

FIGURE 2: Arg82, Asp85, Asp212, and Lys216 with retinal in the ground state of BR shown in three conformations differing in the distance of the guanidinium group of Arg82 to the Schiff base nitrogen. (a) distance 11.5 Å, (b) distance 7.5 Å, (c) distance 4.5 Å.

MATERIALS AND METHODS

(a) The Ground State. For the investigation of the all-trans state, we performed three simulations with a monomer of BR in vacuum and one considering a trimer of BR with lipids, external water, and periodic boundaries, additionally, we analyzed the simulations of Edholm et al. (1995). As initial structure, we used the same as Edholm et al., but without rotating Arg82 toward Asp85 instead keeping Arg82 to point toward the extracellular side as described by Henderson et al. (1990). The difference between the two initial structures is the distance between Arg82 and the SB being 7.5 Å in the simulations of Edholm et al. (1995) and 11.5 Å in our simulations (see Figure 2a,b). So finally, we started our simulations of the all-trans state with the coordinates of the model structure of Henderson et al. (1990) in the helical parts of BR (apart from helix D which was shifted 3 Å toward the cytoplasma) with closed loops and with added termini. To describe the electrostatics within the protein as good as possible, the protonation states of the

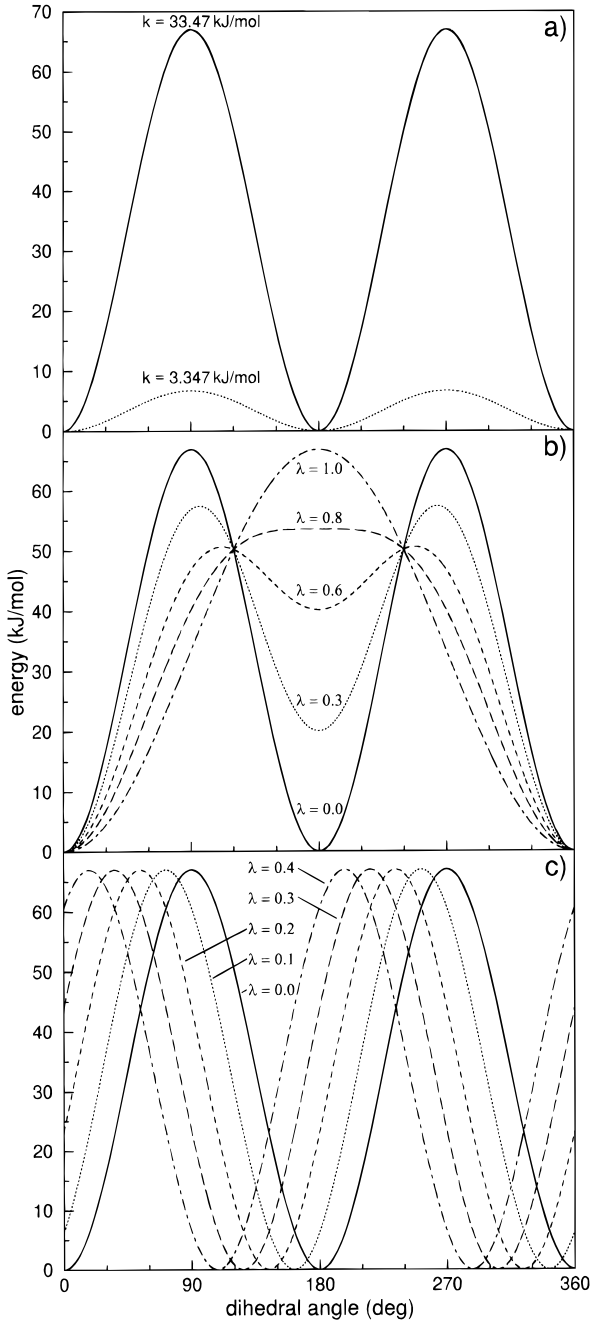

FIGURE 3: (a) Unperturbed dihedral potential in the retinal (—) and dihedral potential with lower energy barrier (method 1, ···). (b) Unperturbed dihedral potential in the retinal (—) and perturbed dihedral potentials in which the minimum at 180° (trans) is deleted (method 2), shown with increasing perturbation parameter λ. (c) Unperturbed dihedral potential in the retinal (—) and perturbed dihedral potentials in which the minimum at 180° is shifted to 0° (method 3), shown with increasing perturbation parameter λ. The potentials for $\lambda = 0$ and $\lambda = 1$ are identical.

internal residues were adopted from experiment. It is known that in the ground state of BR Asp96 and Asp115 are protonated, Asp85 and Asp212 are deprotonated, and the Schiff base nitrogen at Lys216 is protonated (Oesterhelt et al., 1992). Therefore, the carboxyl groups of Asp85 and Asp212 are treated as negatively charged, the SB nitrogen as positively charged by a hydrogen atom, and also Arg82 as positively charged by a hydrogen atom to ensure overall neutrality of the protein interior. Five water molecules were inserted inside the BR molecule between helices C and G as indicated by neutron scattering data (Papadopoulos et al., 1990). One of them was positioned close to the SB group as specified by Raman data (Hildebrandt & Stockburger, 1984). The water molecules were described by the SPC model. For the simulations of a monomer in vacuum, we dealt only with the first 235 amino acids, for the simulations of the trimer with lipids, external water, and periodic boundaries, we considered all the 248 amino acids. The 27 Asp, Glu, Arg, or Lys residues which occur in the peripheral loops and the two chain termini were treated as uncharged in the vacuum simulations and as charged in the presence of external water.

We performed the MD simulations in the same way as Edholm et al. did, i.e., 25 ps strong harmonic restraining to the model structure of Henderson et al. (1990), weakening of the restraining in 10 MD runs of 5 ps each, 25 ps equilibration without any restraining, followed by a production run of 500 ps. We performed three different runs for the monomer in vacuum starting with different initial velocities for the atoms and one simulation of the trimer in water where we could examine each monomer. For more details about the initial structures and the simulations, see Edholm et al. (1995).

(b) Isomerization of the Retinal. The isomerization studies were performed with initial structures taken from the simulations of the BR monomer in vacuum from Edholm et al. (1995). Two different sets of conformations, each consisting of five different structures were used. In set A, the distance between the guanidinium group of Arg82 and the SB nitrogen was approximately 4.5 Å, whereas in set B the distance was roughly 7.5 Å (Figure 2b,c). In the following, these structures are described as $A_{\mathrm{trans},i}$ and $B_{\mathrm{trans},i}$ ($i = 1, ..., 5$) for set A and B, respectively.

Dihedral potentials in the retinal are described in the following way:

$$V(\varphi) = k[1 + \cos(2\varphi - \pi)]$$

with $k = 33.47$ kJ/mol (Figure 3a, solid line). The minima are at $\varphi = 0°$ (cis) and at $\varphi = 180°$ (trans). In order to examine the different retinal conformations, we had to isomerize dihedrals within the chromophore from trans to cis. Three methods were used.

Method 1. Decrease of the force constant k by a factor of 10 (Figure 3a, dotted line) to $k = 3.347$ kJ/mol, resulting in barrier that is only about 2.5 times higher than thermal energy.

Method 2. The dihedral potential

$$V(\varphi) = k[1 + \cos(2\varphi - \pi)]$$

is replaced by

$$V(\varphi, \lambda) = k[1 + \cos(2\varphi - \pi) + \lambda\{\cos(\varphi - \pi) - \cos(2\varphi - \pi)\}]$$

so that the minimum at 180° is deleted with increasing perturbation parameter λ. For $\lambda > 0.8$, the minimum disappears and the dihedral isomerizes to the cis state (Figure 3b).

Method 3. The dihedral potential

$$V(\varphi) = k[1 + \cos(2\varphi - \pi)]$$

is replaced by

$$V(\varphi, \lambda) = k[1 + \cos(2\varphi - (1 - 2\lambda)\pi)]$$

so that the minimum at 180° is shifted to 0° with increasing perturbation parameter λ (Figure 3c).

In method 1, the system decides which state is preferable, because the barrier can be easily passed during the simulation. In methods 2 and 3, the dihedral is forced from the trans to the cis state. The two methods differ by the way that the cis state is reached. The advantage of method 2 compared to method 3 is that less constraints are defined to the system, e.g., the direction or the velocity of rotation. The advantage of method 3 is the possibility of fixing the system in an intermediate state, e.g., at 90°. Besides, the definition of the velocity of isomerization makes it possible to isomerize very slowly, i.e., almost in the thermodynamic equilibrium. This is necessary for the calculation of free energy (Edholm & Ghosh, 1993).

The simulations with the nonpurposive perturbation potential (method 1) were performed by decreasing the energy barrier of the dihedrals $C_{15}-N$, $C_{14}-C_{15}$, $C_{13}-C_{14}$, $C_{12}-C_{13}$, and $C_{11}-C_{12}$ simultanously for 5 ps followed by 1 ps equilibration with normal dihedral potential in order to force the dihedrals either to the cis or to the trans state. These simulations are called $A_{NP,i}$ and $B_{NP,i}$ ($i = 1, ..., 5$) for set A and B, respectively. Isomerization of the retinal with this method allows to investigate the hindrance of rotation of the retinal due to its protein environment. In order to differ between constraints by the protein environment and by retinal itself, we repeated the same simulations with lysine and retinal in vacuum (without the rest of BR). These MD runs are described as $A_{retNP,i}$ and $B_{retNP,i}$ ($i = 1, ..., 5$) in the following.

In the simulations with purposive perturbation potential, we isomerized the retinal to the $C_{13}-C_{14}$ cis, $C_{15}-N$ syn state ($A_{syn,i}$ and $B_{syn,i}$), to the $C_{13}-C_{14}$ cis state ($A_{cis,i}$ and $B_{cis,i}$), and to the $C_{13}-C_{14}$, $C_{14}-C_{15}$ dicis state ($A_{dicis,i}$ and $B_{dicis,i}$) using method 2. Isomerizations in the simulations $A_{dicis,i}$, $B_{dicis,i}$, $A_{syn,i}$, and $B_{syn,i}$ were performed by perturbing the dihedrals simultanously. We set $\lambda = 1$ for 5 ps, followed by 5 ps equilibration with $\lambda = 0$. Isomerization to the $C_{13}-C_{14}$ cis state was also perfomed using method 3 (simulations $A_{m3,cis,i}$ and $B_{m3,cis,i}$). We increased λ from 0 to 1 in 100 ps, then we decreased λ back to 0 within the same time.

(c) Modeling of the M-Intermediate. The modeling of the M-intermediate was started with the 10 structures obtained at the end of the isomerization to $C_{13}-C_{14}$ cis using method 2, $A_{cis,i}$ and $B_{cis,i}$. We changed the topology by deprotonating the SB nitrogen and protonating Asp85 instead. Then we performed a short energy minimization of 50 steps in order to relax local stress. The resulting structures were equilibrated by means of a MD run for 100 ps ($A_{M,i}$ and $B_{M,i}$).

(d) MD Simulations. The MD simulations were performed using the GROMOS package (BIOMOS B.V., University of Groningen, Groningen, Netherlands). In all simulations, SHAKE was used for bond length restraining (Ryckaert et al., 1977) and the temperature was kept at 300 K by coupling the systems to an external heat bath (Berendsen et al., 1984) with a time constant of 0.1 ps. The time step used in the simulations was 2 fs. The nonbonded interactions were cutoff at 10 Å and a neighbor list technique was used with updates every 10 steps. The simulations were performed on DEC 3000-300LX and DEC 3000-800 workstations and took for BR 0.15 cpuh/ps (monomer in vacuum) and 3.3 cpuh/ps (trimer in water), respectively.

Table 1: Root-Mean-Square Deviations between the MD Structures of Our Simulations and the Two Model Structures (Henderson et al., 1990; Grigorieff et al., 1996)

simulation[a]	rmsd (Å)[b]	rmsd (Å)[c]	rmsd (Å)[d]
monomer in vacuum, run 1	1.4	1.2	2.4
monomer in vacuum, run 2	1.5	1.4	2.8
monomer in vacuum, run 3	1.5	1.3	2.4
trimer in water, monomer 1	1.8	1.7	3.1
trimer in water, monomer 2	1.8	1.7	3.3
trimer in water, monomer 3	1.8	1.8	3.3

[a] A time average over 300 ps was performed for each simulation. [b] Rmsd to the backbone atoms of the helical parts of Henderson et al. (1990). [c] Rmsd to the backbone atoms of the helical parts of Grigorieff et al. (1996). [d] Rmsd to the backbone atoms of the helical parts and the loops of Grigorieff et al. (1996).

RESULTS

(a) The Ground State. As a control for the quality of our simulations, we calculated the r.m.s deviation to the model structure (Henderson et al., 1990, with helix D shifted 3 Å) and to the refined model structure (Grigorieff et al., 1996). The two first columns in Table 1 show the values for the backbone atoms of the helical parts of BR. With a rms deviation of approximately 1.5 Å for the monomer and 1.8 Å for the trimer simulations, the MD structures stayed close to their initial conformation, the model structure of Henderson et al. (1990). Surprisingly, the rms deviation was even slightly lower in comparison to the refined model structure (Grigorieff et al., 1996). In the third column of Table 1, the interhelical loops are also considered. These values are clearly higher because of the poor quality and the large fluctuations of the loop structures. The higher rms deviation of each monomer in the trimer simulation has already been observed by Edholm et al. (1995). The three monomers do not behave identical, averaging of the ensemble improves the result to 1.3 Å.

For the simulations of the monomer in vacuum, the distance between Arg82 and the SB, which we defined as the shortest distance of one H-atom of the guanidinium group to the SB nitrogen, remained between 11 and 12 Å during the strong harmonic restraining of the first 25 ps MD run. With decreasing restraining potential, this distance lowered rapidly, so that the value of about 7.5 Å with which Edholm et al. began their simulations was already reached after 50 ps, although there was still a weak restraining potential toward coordinates of the model structure of Henderson et al. (1990). In this position, Arg82 was quite stable, but finally, by passing a metastable intermediate with a distance of 5.5−6 Å, it rotated further toward the SB to approximately 4.5 Å (data not shown). We observed a similar behavior of the Arg82 side chain in the simulation of the trimer. The trajectory of the distance between Arg82 and the SB is shown in Figure 4, for each monomer separately. At the beginning of the production run, Arg82 already reached a position which was close to the starting structure of Edholm et al. (1995), although we tried to avoid a rotation of Arg82 toward the SB by using a restraining potential. During the production run, two stable states for Arg82, one at a distance of 7.5 Å and one at a distance of 4.5 Å to the SB were observed. At the end of the simulations, however, all three monomers were captured in the 4.5 Å state, because once the 4.5 Å state was reached, a reorientation of Arg82 back to 7.5 Å did not occur. The preference for the 4.5 Å state may be

Table 2: Orientation of the Retinal Described by Means of Different Angles in the All-Trans State, the $C_{13}-C_{14}$ cis, $C_{15}-N$ syn State (syn), the $C_{13}-C_{14}$ cis State (cis), the $C_{13}-C_{14,}$ $C_{14}-C_{15}$ Dicis State (dicis), and in the M-Intermediate (M) Compared to Experimental Data[a]

	angle (deg)												
	all-trans				syn		cis		dicis		M		
specification	initial	MDA	MDB	exp	MDA	MDB	MDA	MDB	MDA	MDB	MDA	MDB	exp
C_6-C_{14}-*n*	117	119	114	121[b]	125	120	127	122	132	127	128	124	
Hauss et al.	22	41	35	39[c]	46	42	48	44	51	48	49	46	49[c]
$C_{20}-C_{13}-n$	54	24	18	32[d]	27	21	34	28	46	35	33	31	
$C_{19}-C_9-n$	35	42	31	42[d]	42	34	44	35	48	38	45	41	44[e]
$C_{18}-C_5-n$	4	32	24	37[d]	31	26	32	24	32	25	35	30	

[a] The angle specifications $C_6-C_{14}-n$, $C_{20}-C_{13}-n$, $C_{19}-C_9-n$, and $C_{18}-C5-n$ describe the angles between the corresponding atoms and the membrane normal *n*. Hauss et al. describes an angle between the membrane plane and a vector defined by Hauss et al. (1994) (vector between the center of mass (CM) of five ^{2}H-labels near the SB and the CM of 11 ^{2}H-labels in the β-ionone ring). Initial are the values of our starting conformation (Henderson et al., 1990) and of the 11.5 Å conformation in our simulations. MDA and MDB are the results of the simulations of set A and B, respectively, the analyzed MD structures are time averaged over 20 ps and ensemble averaged over five runs. The column exp shows various experimental data. [b] ECM data of Grigorieff et al. (1996). [c] Neutron diffraction data of Hauss et al. (1994). [d] ^{2}H-NMR data of Ulrich et al. (1994). [e] ^{2}H-NMR data of Ulrich et al. (1995).

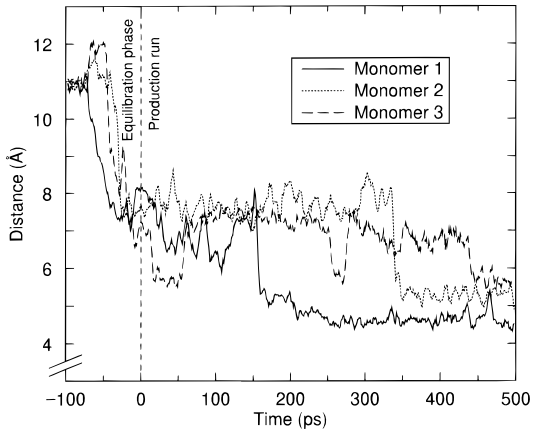

FIGURE 4: Temporal variation of the distance between Arg82 and the SB, defined as the shortest distance of one H-atom of the guanidinium group to the SB nitrogen, during the simulation of a trimer in water. The simulation started with a restraining and equilibration phase of 100 ps, the production run extended from 0 to 500 ps.

due to the gain of energy of about 150 kJ/mol. These findings are in agreement to the simulations of Edholm et al. (1995).

In the further investigations, we focused on the 7.5 Å and the 4.5 Å conformations. The 11.5 Å state was not longer considered, because of its instability and the results of the p*K* calculations of Bashford and Gerwert (1992). In addition, comparison of the retinal orientation with ^{2}H-NMR data (Ulrich et al., 1994) and neutron diffraction data (Hauss et al., 1994) supported this decision (Table 2).

In Table 2, we compared the retinal orientation from our simulations to several experimental data. The angles for set A (distance between Arg82 and SB 4.5 Å) and B (distance 7.5 Å) are averaged values from the structures $A_{trans,i}$ and $B_{trans,i}$ ($i = 1, ..., 5$), respectively. During the simulations, the angles changed from the values of the initial conformation (Henderson et al., 1990) to values which are in agreement to newer ECM data (Grigorieff et al., 1996), ^{2}H-NMR data (Ulrich et al., 1994), and neutron diffraction data (Hauss et al., 1994). The angles of set A agreed better to the experimental data than those of set B, which were too low. We observed a small overall twist along the chromophore of approximately 15° between the chain planes at C_6 and C_{14} which had been described before (Edholm et al., 1995). This is in agreement to experimental results (Fahmy et al., 1989), but at variance with the MD simulations of Humphrey et al. (1994) who obtained a large twist of about 60°.

Table 3: Number of Occurrence of Different States of the Retinal with and without BR at the End of Our Simulations with Nonpurposive Isomerization of the Dihedrals $C_{15}-N$, $C_{14}-C_{15}$, $C_{13}-C_{14}$, $C_{12}-C_{13}$, and $C_{11}-C_{12}$[a]

	number of occurrence		
state of the retinal	$A_{NP,i}$	$B_{NP,i}$	$A_{retNP,i}$, $B_{retNP,i}$
all-trans	2		
$C_{12}-C_{13}$ cis			2
$C_{13}-C_{14}$ cis	1		3
$C_{15}-N$ syn			1
$C_{12}-C_{13,}$ $C_{14}-C_{15}$ dicis			1
$C_{12}-C_{13}$ cis, $C_{15}-N$ syn			1
$C_{13}-C_{14}$, $C_{14}-C_{15}$ dicis			2
$C_{13}-C_{14}$ cis, $C_{15}-N$ syn	2	5	

[a] In the columns $A_{NP,i}$ and $B_{NP,i}$, the results of the simulations in BR are shown for set A and B, respectively. In the third column, the results of set A and B are taken together, because we only considered the retinal in vacuum in these simulations. [b] Nonpurposive isomerization was performed by decreasing the energy barrier of the dihedral potentials simultanously (method 1).

(b) Isomerization of the Retinal. In the following, we present the results of the investigation of other retinal states, starting from the conformations $A_{trans,i}$ and $B_{trans,i}$ ($i = 1, ..., 5$). Since the simulations of the monomer and trimer with the all-trans chromophore resulted in very similar overall structures in general and retinal orientations in particular, all the isomerizations on the retinal were done on monomers.

(b1) Nonpurposive Isomerization of the Dihedrals $C_{15}-N$, $C_{14}-C_{15}$, $C_{13}-C_{14}$, $C_{12}-C_{13}$, and $C_{11}-C_{12}$ in the Retinal. In the simulations $A_{NP,i}$ and $B_{NP,i}$, we examined which isomerizations are sterically allowed due to the environmental protein by lowering the energy barrier in the dihedral potential. Table 3 shows the results of the MD runs. Only three different states were observed in the 10 simulations of the retinal in BR (Table 3, column 1 and 2), the all-trans state, the $C_{13}-C_{14}$ cis state, and the $C_{13}-C_{14}$ cis, $C_{15}-N$ syn state. These are the same dihedrals in which isomerization was observed in experiments (Braiman & Mathies, 1980; Smith et al., 1984, 1986). The dihedrals $C_{11}-C_{12}$, $C_{12}-C_{13}$ and $C_{14}-C_{15}$ stayed in the trans state in each simulation. Though the rms fluctuations around 180° for these three dihedrals increased to 26° under perturbation compared to 13° under normal conditions, no transition occurred. Obviously, the $B_{NP,i}$ structures showed a preference for the $C_{13}-C_{14}$ cis, $C_{15}-N$ syn state, whereas the occurrence of the states in the $A_{NP,i}$ simulations was quite balanced.

Table 4: Energy Differences ΔE^a of the Isomerized States Compared to the All-Trans State[b]

retinal conformation	ΔE (kJ/mol) MDA[c]	MDB
$C_{13}-C_{14}$ cis	+24	−10
$C_{13}-C_{14}$, $C_{14}-C_{15}$ dicis	+58	+32
$C_{13}-C_{14}$ cis, $C_{15}-N$ syn	−0.4	−5.2

[a] $\Delta E = E$(isomerized) − E(all-trans). [b] The values are an average over the simulations using the purposive isomerization method 2. [c] MDA and MDB are the results of the simulations of set A and B, respectively.

In order to distinguish between constraints by the retinal itself and the protein environment, the same MD runs were repeated with lysine and retinal in vacuum in the simulations $A_{retNP,i}$ and $B_{retNP,i}$. The results showed that the retinal itself has more possibilities to isomerize than retinal in BR, but not each dihedral was observed to isomerize (Table 3, column 3). The least stable dihedrals are $C_{13}-C_{14}$ and $C_{12}-C_{13}$, because isomerization of these dihedrals does not cause any steric hindrance between the atoms of the retinal. The transition to cis did not occur in the dihedral $C_{11}-C_{12}$, because of steric interactions between the retinal chain and the methyl group at C_{20}.

Finally, we want to emphasize, that isomerization around the dihedral $C_{14}-C_{15}$ did not occur in any of the nonpurposive isomerizations $A_{NP,i}$ and $B_{NP,i}$, also it did so in the simulations $A_{retNP,i}$ and $B_{retNP,i}$, i.e., this dihedral is thus tightly fixed by its environment in BR.

(b2) Purposive Isomerization of the Retinal to the $C_{13}-C_{14}$ cis, $C_{15}-N$ syn State, the $C_{13}-C_{14}$ cis State, and the $C_{13}-C_{14}$, $C_{14}-C_{15}$ Dicis State. The simulations $A_{syn,i}$ and $B_{syn,i}$ were performed in order to investigate the quality of the description of the retinal environment. The $C_{13}-C_{14}$ cis, $C_{15}-N$ syn state as part of the dark-adapted state is expected to have a similar, but slightly lower energy than the all-trans state, because of the experimentally found mixture ratio of 2:1 (Scherrer et al., 1989; Song et al., 1995). From the mixture ratio one may calculate a free energy difference using the Boltzmann distribution $N(BR_{555})/N(BR_{568}) = e^{\Delta F/kT}$. This gives $\Delta F = 1.7$ kJ/mol in favor of the BR_{555} state. The simulations give small energy and free energy differences that are compatible with this experimental finding, the agreement is slightly better for set A (Table 4). The statistical uncertainties in energy and free energy data are however too large to make a quantitative comparison meaningful. Nevertheless, this result shows that the quality of the description of the retinal environment is quite good and that energetic considerations give sensible results. Visual inspection of the structures showed that there was nearly no difference between the all-trans and the $C_{13}-C_{14}$ cis, $C_{15}-N$ syn state. The two dihedrals just performed a kind of pedal motion without much influence on their environment. The angle between the retinal and the membrane normal slightly increased as shown in Table 2.

Isomerization to the $C_{13}-C_{14}$ cis state and the $C_{13}-C_{14}$, $C_{14}-C_{15}$ dicis state (simulations $A_{cis,i}$, $B_{cis,i}$, $A_{dicis,i}$, and $B_{dicis,i}$) were performed in order to model the first steps of the BR photocycle. In the simulations to $C_{13}-C_{14}$ cis ($A_{cis,i}$ and $B_{cis,i}$), the isomerized state was reached in all cases, whereas isomerizations to the $C_{13}-C_{14}$, $C_{14}-C_{15}$ dicis state were successful only in eight out of 10 attempts. Simulation $A_{dicis,3}$ ended in the $C_{13}-C_{14}$ cis state and simulation $B_{dicis,2}$ reached a $C_{14}-C_{15}$ cis conformation. The successful conversions of the $C_{13}-C_{14}$, $C_{14}-C_{15}$ dicis state were also slower than the other isomerizations. The experimental finding of a positive charge shift toward the inner side of the membrane of approximately 1.5 Å in the early intermediates of the photocycle (Keszethelyi & Ormos, 1980) was only observed in the conversions to the $C_{13}-C_{14}$ cis state, but not in the conversions to the $C_{13}-C_{14}$, $C_{14}-C_{15}$ dicis state. The isomerization in the retinal dihedrals was in both cases compensated by dihedral changes in the lysine side chain. These changes were, however, larger in the dicis case. Table 2 shows the orientation of the retinal for the two states as resulted from our simulations. The angle between the vector C_6-C_{14} and the membrane normal increased by 8° compared to the all-trans state during isomerzation to $C_{13}-C_{14}$ cis and by at least 12° during isomerization to the $C_{13}-C_{14}$, $C_{14}-C_{15}$ dicis state. Assuming that the orientation of the transition dipole moment can be described by this angle, the result for $C_{13}-C_{14}$ cis is in perfect agreement to experiments of Esquerra et al. (1996), who obtained an increase of 8° in the first steps of the photocycle. As in the ground state, the angles presented in Table 2 are larger for set A than for set B. The energy differences of the $C_{13}-C_{14}$ cis and the $C_{13}-C_{14}$, $C_{14}-C_{15}$ dicis state compared to the all-trans state are shown in Table 4. As expected, the energy of the $C_{13}-C_{14}$, $C_{14}-C_{15}$ dicis state is higher for the structures of set A and B, the difference is bigger for the set A conformations. An interesting result was found for the $C_{13}-C_{14}$ cis structures. Whereas for set A structures the $C_{13}-C_{14}$ cis state had a higher energy than the all-trans state, the result for set B showed a contrary behavior. For further investigation, the free energy difference between the $C_{13}-C_{14}$ cis and the all-trans state was calculated by integration along a slow (100 ps) isomerization according to method 3. The free energy was approximately 6 kJ/mol higher in the $C_{13}-C_{14}$ cis state compared to the all-trans state in the simulations $A_{m3,cis,i}$ whereas in the simulations $B_{m3,cis,i}$ free energy was about 10 kJ/mol lower in the $C_{13}-C_{14}$ cis state. For both simulations hysteresis and statistical errors were estimated according to Edholm and Ghosh (1993), they permit to give an accuracy of 10 kJ/mol. For set B, we found lower values for the $C_{13}-C_{14}$ cis state compared to the all-trans state in both potential energy and free energy.

We also monitored the change of shape in BR during the isomerization. Figure 5a shows the positions of the seven helices and the contour of BR. The contour is defined as the 30% line of the projected electron density map of the helical part of BR (Figure 5b). Figure 5c shows the typical difference map of the simulations $A_{cis,i}$ compared to the ground state. Overall, no big differences occurred, however a clear density increase was found near Tyr185. A slight outward tilt of the cytoplasmic end of helix F can also be observed. The changes near Tyr185 were smaller and no outward tilt of helix F was observed in the simulations $B_{cis,i}$ (data not shown).

(c) Modeling of the M-Intermediate. We started the modeling of the M-intermediate with the resulting structures of simulation $A_{cis,i}$ and $B_{cis,i}$ which we name L-intermediate, the modeled structures are called $A_{M,i}$ and $B_{M,i}$ in the following.

In nine out of the ten simulations, Arg82 kept its orientation during the equilibration phase, in simulation $B_{M,4}$

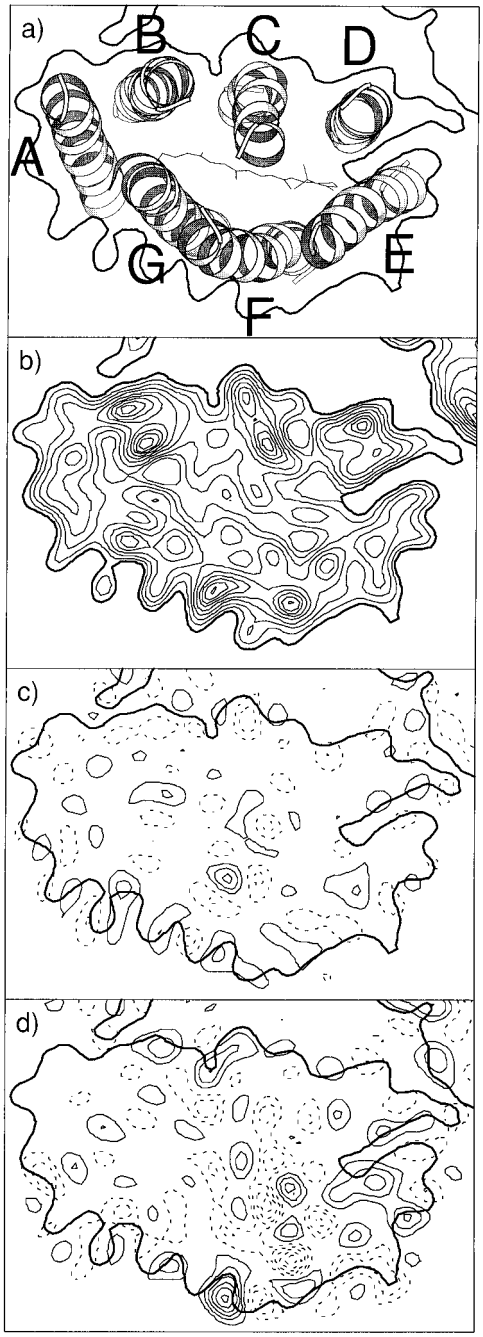

FIGURE 5: (a) Average structure of BR with marked helices created with MOLSCRIPT (Kraulis, 1991) and the contour of BR. (b) Two-dimensinal projection Fourier maps of the helical parts of BR in the ground state, made with the CCP4 program package (Daresbury Laboratory, Warrington, U.K.). The line of 30% density is defined as the contour of BR. (c) Difference Fourier map showing changes in the projected structure between the $C_{13}-C_{14}$ cis and the all-trans state. (d) Difference Fourier map showing changes in the projected structure between the M-intermediate and the all-trans state. In panels c and d, the solid lines show a higher density in the $C_{13}-C_{14}$ cis state and in the M-intermediate, respectively, whereas the dashed lines show negative density differences.

however, the guanidinium group of Arg82 moved closer to the SB to a final distance of approximately 4.5 Å.

Table 2 shows the orientation of the retinal resulted from simulation $A_{M,i}$ and $B_{M,j}$ ($i = 1, ..., 5$; $j = 1, 2, 3, 5$) compared to ^{2}H-NMR (Ulrich et al., 1995) and neutron diffraction data (Hauss et al., 1994). It is obvious that our data are in good agreement to the experimental outcome for set A. The values are again lower for set B, but the difference decreased. In simulation $B_{M,4}$, the results showed the typical set A behavior, e.g., the angle $C_6-C_{14}-n$ was 128° and the angle defined by Hauss et al. (1994) was 50°. Comparison of the values in Table 2 shows that the orientation of the retinal was nearly the same in the simulations $A_{cis,i}$ and $A_{M,i}$.

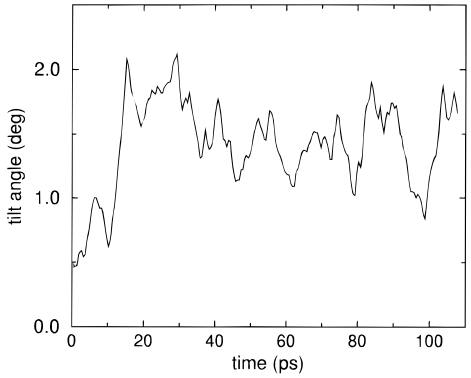

FIGURE 6: Changes in the tilt angle of helix F during isomerization to the $C_{13}-C_{14}$ cis state (0 ps < t < 10 ps) and during formation of the M-intermediate (10 ps < t < 110 ps) compared to the averaged tilt angle of the all-trans state.

The changes in density map as occurred in the simulations $A_{M,i}$ ($i = 1, 2, 4, 5$) and $B_{M,4}$ are shown in Figure 5d. The most conspicious difference to Figure 5c is the increase in the outward tilt of the cytoplasmatic part of helix F which is in agreement with electron diffraction studies of Subramaniam et al. (1993). This outward tilt could not be observed in the other simulations of set B, it was clearly lower in $A_{M,3}$.

In Figure 6, we present the changes of the tilt angle of helix F during formation of the L-intermediate (t < 10ps) and during modeling of the M-intermediate (10 ps < t < 110 ps). It is seen that the main part of the increase in tilt of helix F does not occur during the isomerization part (first 10 ps) of the simulation, but first after deprotonation of the Schiff base and protonation of Asp85.

In contrast to a wide spread assumption (e.g., Scharnagl et al., 1995), we did not observe a motion of the Arg82 side chain but rather of the Asp85 side chain toward the extracellular side during formation of the M-intermediate.

DISCUSSION

The rmsd between the membrane spanning part of our simulated structure and the model structure of BR (Henderson et al., 1990) is very low. The rmsd is even lower (for the membrane spanning part) when our structure is compared to the refined structure (Grigorieff et al., 1996). The loop structures are poor, but we could at least confirm the prediction of MD simulations (Edholm et al., 1995) and the experimental outcome (Grigorieff et al., 1996) that the rms fluctuations in the cytoplasmic loops are higher than on the extracellular side. This encouraged us to investigate the important topic of orientation of Arg82 in different intermediates.

With our simulations, we are able to confirm the suggestion of Bashford and Gerwert (1992) that Arg82 does not point outward in the ground state of BR as described in the model structures based on ECM (Henderson et al., 1990; Grigorieff et al., 1996). The reason for the stabilization of the Arg82 side chain close to the Schiff base may be that in this way the two positive and two negative interior charges gather close to each other. This should clearly be strongly

electrostaticly favored (in a region with low dielectric constant) compared to a structure with one positive charge more than 10 Å away from the other charges. The lower energy and comparison with ^{2}H-NMR and neutron diffraction data (Table 2) even indicate that the distance between the guanidinium group of Arg82 and the SB nitrogen is, with a value of 4.5 Å, lower than suggested by Bashford and Gerwert. This outcome is in agreement to the complex counter ion model (de Groot et al., 1990) which requires a positive charge close to the Schiff base which is not there in the model structures (Henderson et al., 1990; Grigorieff et al., 1996) but is present in the form of the Arg82 side chain in our simulations.

The similarity of the energy difference calculated between the $C_{13}-C_{14}$ cis, $C_{15}-N$ syn and all-trans state and the corresponding energy difference calculated from the experimental mixture ratio between the two isomers in the dark-adapted state supports the simulated structure. The better agreement for set A simulations indicates that Arg82 is located close to the SB in both the all-trans and the $C_{13}-C_{14}$, $C_{15}-N$ syn state. This finding is supported by the simulations $A_{NP,i}$ and $B_{NP,i}$. Whereas the simulations $A_{NP,i}$ showed a balanced occurrence of the $C_{13}-C_{14}$ cis and the $C_{13}-C_{14}$, $C_{15}-N$ syn state, there was a clear preference of the $C_{13}-C_{14}$, $C_{15}-N$ syn state in the MD runs $B_{NP,i}$.

As mentioned above, there are still contradictory opinions about the retinal conformations which are passed in the first steps of the photocycle. Nonella et al. (1991) and Zhou et al. (1993) argued in favor of the existence of a $C_{13}-C_{14}$, $C_{14}-C_{15}$ dicis state, because they observed an easier isomerization to the $C_{13}-C_{14}$, $C_{14}-C_{15}$ dicis state compared to the $C_{13}-C_{14}$ cis state in their MD simulations. In contrast to their results, our simulations using the nonpurposive perturbation potential (method 1) show that the dihedral $C_{14}-C_{15}$ is tightly packed by the environmental protein. Isomerization to the $C_{13}-C_{14}$, $C_{14}-C_{15}$ dicis state occurred slower than isomerization to the $C_{13}-C_{14}$ cis state in the simulations using method 2 (deletion of the minimum at 180°), and in two out of 10 attempts, we were not able to reach the $C_{13}-C_{14}$, $C_{14}-C_{15}$ dicis state. The charge shift toward the inner side of the membrane which was observed in the first steps of the photocycle by measuring the electric signal (Keszthelyi & Ormos, 1980) could only be observed when isomerization to the $C_{13}-C_{14}$ cis state was performed. The strongest argument against the existence of the $C_{13}-C_{14}$, $C_{14}-C_{15}$ dicis state follows from comparison of our results presented in Table 2 with experimental data of Esquerra et al. (1996) who observed an increase in the chromophore's transition dipole moment of less than 8° during the first steps of the photocycle. This result is in agreement to the value of 8° for the $C_{13}-C_{14}$ cis state, but at variance with the larger increase of the $C_{13}-C_{14}$, $C_{14}-C_{15}$ dicis state of 12°. So we agree with the C-T model, proposed by Fodor et al. (1988) on the basis of resonance Raman data and find only evidence against the occurrence of the $C_{13}-C_{14}$, $C_{14}-C_{15}$ dicis state in the early stages of the photocycle.

The energy and free energy of all the structures $A_{cis,i}$ showed a higher value than the corresponding structures $A_{trans,i}$. Unlike that, the results for the simulations $B_{cis,i}$ were completely different, with energy and free energy in the $C_{13}-C_{14}$ cis state being lower than in the all-trans state. Because the values for energy as well as for free energy should be higher for the excited state compared to the ground state, we judge this outcome as an indication for the location of Arg82 close to the SB, at a distance of about 4.5 Å.

Although there exist no experimental data on the retinal orientation in the early intermediates of the photocycle and in the $C_{13}-C_{14}$ cis, $C_{15}-N$ syn state, we present the outcome of our simulations in Table 2. We hope that in the future experimentally determined orientational data will be available which could be compared to the values in Table 2.

The results of our simulations of the M-intermediate of the photocycle argue for the location of Arg82 close to the SB, too, because the orientation of the retinal in our M-intermediates agreed well to ^{2}H-NMR (Ulrich et al., 1995) and to neutron diffraction data (Hauss et al., 1994) for the simulations $A_{M,i}$. The values for $B_{M,i}$ were again too low. The outward tilt in the cytoplasmic end of helix F could only be observed in $A_{M,i}$ and $B_{M,4}$, but not in the other $B_{M,i}$. In $B_{M,4}$, however, the side chain of Arg82 rotated toward the SB during formation of the M-intermediate, so that we have to consider it as a 4.5 Å conformation. The size of the outward tilt of the cytoplasmic part of helix F is much lower in our simulations than described by Xu et al. (1995), but it is in agreement with the ECM data of Subramaniam et al. (1993).

A very interesting observation was that in simulation $B_{M,4}$ helix F tilted outwards, but only after that the Arg82 side chain had moved closer from its original distance of 7.5 Å to the SB. So, correlated motions across large distances inside BR do occur. Another example, which is easy to understand, is the correlation between the tilt of the retinal and the distance between the Arg82 side chain and the retinal. In the absence of the positively charged Arg82, the also positively charged SB must shield the two negative amino acids Asp85 and Asp212 from each other. By rotating toward the SB, Arg82 partially takes over the role of shielding the two negatively charged residues and the SB is repelled toward the cytoplasm, so that the angle between the retinal and the membrane normal increases. We assume that the retinal motion is mediated to helix F via Trp182 or Tyr185. In fact, Figure 5c shows a change in density at Tyr185 caused by retinal isomerization. However, further investigations will be necessary to check whether more residues show a correlated behavior and in which manner these correlations play a role in the photocycle.

It is assumed that water penetrates in the pore opened by the outward tilt of helix F which finally builds a water chain between Asp96 and the SB (Subramaniam et al., 1993; Brown et al., 1995a). Because we only simulated BR in vacuum, we could not observe the penetration of water, but we hope that this will be possible in future simulations of the M-intermediate with external water.

In spite of big efforts, the proton release group could not be identified for many years. Scharnagl et al. (1994, 1995) proposed Glu204 to be the proton release group and recent FTIR studies of Brown et al. (1995b) seem to confirm their proposal. Scharnagl et al. proposed furthermore that orientation of Arg82 toward the extracellular side changes the p*K* of Glu204 and induces deprotonation. We did not observe this, the positively charged Arg82 stayed closely at the negatively charged Asp212 in the M-intermediate. We only observed orientation of the now protonated Asp85 toward the outside of the membrane. But if Glu204 is really the proton release group, Asp85 is too far away to induce its deprotonation directly. Perhaps a water chain between

Glu204 and Asp85 which could bridge the distance can be formed when the protonated Asp85 rotates in the extracellular direction. Future simulations considering more water are necessary to check this idea.

The high accuracy of our simulations compared to experimental data allows us to propose that Arg82 points toward the inner side of the membrane, located even closer to the SB than predicted by Bashford and Gerwert (1992). The guanidinium group is stable at this position in the $C_{13}-C_{14}$ cis, $C_{15}-N$ syn state as part of the dark-adapted state and in the course of the photocycle at least until formation of the M-intermediate. Furthermore, we found no evidence for that the retinal has a $C_{13}-C_{14}$, $C_{14}-C_{15}$ dicis conformation in the K/L-intermediates of the photocycle, but our results support the C-T model of Fodor et al. (1988).

REFERENCES

Balashov, S. P., Govindjee, R., Kono, M., Imasheva, E., Lukashev, E., Ebrey, T. G., Crouch, R. K., Menick, D. R., & Feng, Y. (1993) *Biochemistry 32*, 10331−10343.

Bashford, D., & Gerwert, K. (1992) *J. Mol. Biol. 224*, 473−486.

Berendsen, H. J. C., Postma, J. P. M., van Gunsteren, W. F., DiNiola A., & Haak, J. R. (1984) *J. Chem. Phys. 81*, 3684−3690.

Birge, R. R. (1990) *Biochim. Biophys. Acta 1016*, 293−327.

Braiman, M. S., & Mathies, R. (1980) *Biochemistry 19*, 5421−5428.

Brown, L. S., Váró, G., Needleman, R., & Lanyi, J. K. (1995a) *Biophys. J. 69*, 2103−2111.

Brown, L. S., Sasaki, J., Kandori, H., Maeda, A., Needleman, R., & Lanyi, J. K. (1995b) *J. Biol. Chem. 270* (N45), 27122−27126.

Edholm, O., & Ghosh, I. (1993) *Mol. Simul. 10*, 241−253.

Edholm, O., Berger, O., & Jähnig, F. (1995) *J. Mol. Biol. 250*, 94−111.

Engels, M., Gerwert, K., & Bashford, D. (1995) *Biophys. Chem. 56*, 95−104.

Esquerra, R. M., Che, D., Shapiro, D. B., Lewis, J. W., Bogomolni, R. A., Fukushima, J., & Kliger, D. (1996) *Biophys. J. 70*, 962−970.

Fahmy, K., Siebert, F., Grossjean, M. F., & Tavan, P. (1989) *J. Mol. Struct. 214*, 257−288.

Fahmy, K., Weidlich, O., Engelhard, M., Sigrist, H., & Siebert, F. (1993) *Biochemistry 32*, 5862−5869.

Fodor, S. P. A., Ames, J. B., Gebhard, R., van den Berg, A. M. M., Stoeckenius, W., Lugtenburg, J., & Mathies, R. A. (1988) *Biochemistry 27*, 7097−7101.

Grigorieff, N., Ceska, T. A., Downing, K. H., Baldwin, J. M., & Henderson, R. (1996) *J. Mol. Biol. 259*, 393−421.

de Groot, H. J. M., Smith , S. O., Courtin, J., van den Berg, E., Winkel, C., Lugtenburg, J., Griffin, R. G., & Herzfeld, J. (1990) *Biochemistry 29*, 6873-6883.

Hauss, T., Büldt, G., Heyn, M. P., & Dencher, N. A. (1994) *Proc. Natl. Acad. Sci. U.S.A. 91*, 11854−11858.

Hessling, B., Souvignier, G., & Gerwert, K. (1993) *Biophys. J. 65*, 1929−1941.

Henderson, R., Baldwin, J. M., Ceska, T. A., Zemlin, F., Beckmann, E., & Downing, K. H. (1990) *J. Mol. Biol. 213*, 899−929.

Hildebrandt, P., & Stockburger, M. (1984) *Biochemistry 23*, 5539−5548.

Humphrey, W., Logunov, I., Schulten, K., & Sheves, M. (1994) *Biochemistry 33*, 3668−3678.

Keszthelyi, L., & Ormos, P. (1980) *FEBS Lett. 109*, 189−193.

Kraulis, P. (1991) *J. Appl. Crystallogr. 24*, 946−950.

Mathies, R. A., Lin, S. W., Ames, J. B., & Pollard, W. T. (1991) *Annu. Rev. Biophys. Chem. 20*, 491−518.

Nonella, M., Windemuth, A., & Schulten, K. (1991) *Photochem. Photobiol. 54*, 937-948.

Oesterhelt, D., Tittor, J., & Bamberg, E. (1992) *J. Bioenerg. Biomembr. 24*, 181−191.

Papadopoulos, G., Dencher, N., Zaccai, G., & Büldt, G. (1990) *J. Mol. Biol. 214*, 15−19.

Ryckaert, J.-P., Ciccotti, G., & Berendsen, H. J. C. (1977) *J. Comput. Phys. 23*, 327−341.

Scharnagl, C., Hettenkofer, J., & Fischer, S. F. (1994) *Int. J. Quantum Chem., Quantum Biol. Symp. 21*, 33−56.

Scharnagl, C., Hettenkofer, J., & Fischer, S. F. (1995) *J. Phys. Chem. 99*, 7787−7800.

Scherrer, P., Mathew, M. K., Sperling, W., & Stoeckenius, W. (1989) *Biochemistry 28*, 829−834.

Schulten, K., Schulten, Z., & Tavan, P. (1984) Info and Energy Transd. in Biol. Membr. pp 113−131. Alan R. Liss, Inc., New York.

Smith, S. O., Myers, A. B., Pardoen, J. A., Winkel, C., Mulder, P. P. J., Lugtenburg, J., & Mathies, R. A. (1984) *Proc. Natl. Acad. Sci. U.S.A. 81*, 2055−2059.

Smith, S. O., Hornung, I., van der Steen, R., Pardoen, J. A., Braiman, M. S., Lugtenburg, J., & Mathies, R. A. (1986) *Proc. Natl. Acad. Sci. U.S.A. 83*, 967−971.

Song, L., Yang, D., El-Sayed, M. A., & Lanyi, J. K. (1995) *J. Phys. Chem. 99*, 10052−10055.

Subramaniam, S., Gerstein, M., Oesterhelt, D., & Henderson, R. (1993) *EMBO J. 12*, 1−8.

Ulrich, A. S., Wallat, I., Heyn, M. P., & Watts, A. (1994) *Biochemistry 33*, 5370−5375.

Ulrich, A. S., Wallat, I., Heyn, M. P., & Watts, A. (1995) *Nat. Struct. Biol. 2*, 190−192.

Xu, D., Sheves, M., & Schulten, K. (1995) *Biophys. J. 69*, 2745−2760.

Zhou, F., Windemuth, A., & Schulten, K. (1993) *Biochemistry 32*, 2291−2306.

BI962427H